atoms

MDPI

Article

Ionization of Helium by Proton Impact in a Quasi-Sturmian Approach Built upon the 3C Model

Sergey A. Zaytsev [1], Darya S. Zaytseva [1], Alexander S. Zaytsev [1], Lorenzo U. Ancarani [2,*], Konstantin A. Kouzakov [3,4] and Yury V. Popov [5,6]

[1] Laboratory for Modeling of Quantum Processes, School of Fundamental and Computer Sciences, Pacific National University, 680035 Khabarovsk, Russia; zaytsevsa@pnu.edu.ru (S.A.Z.); 2012002939@pnu.edu.ru (D.S.Z.); alzaytsev@pnu.edu.ru (A.S.Z.)
[2] CNRS, Laboratoire de Physique et Chimie Théoriques, Université de Lorraine, 57000 Metz, France
[3] Department of Nuclear Physics and Quantum Theory of Collisions, Faculty of Physics, Lomonosov Moscow State University, 119991 Moscow, Russia; kouzakov@srd.sinp.msu.ru
[4] Department of Physics, Branch of Lomonosov Moscow State University in Sarov, 607328 Sarov, Russia
[5] Skobeltsyn Institute of Nuclear Physics, Lomonosov Moscow State University, 119991 Moscow, Russia; popov@srd.sinp.msu.ru
[6] Bogoliubov Laboratory of Theoretical Physics, Joint Institute for Nuclear Research, 141980 Dubna, Russia
* Correspondence: ugo.ancarani@univ-lorraine.fr

Abstract

We investigate theoretically the 75 keV proton-impact ionization of atomic helium. The convoluted quasi-Sturmian approach is extended to treat, on an equal footing, both the direct mechanism and the electron capture to the continuum. This is achieved by proposing an ansatz of the Green's function of the three-body Coulomb system $(e^-, \mathrm{He}^+, p^+)$ that is compatible with the well-known 3C correlated continuum wave function. The model that stems from this approximation, named 3$\tilde{\mathrm{C}}$, is tested numerically using parabolic Sturmian expansions. Calculations of fully differential cross sections are presented for different regimes of energy losses, namely for ejected electron energies below, nearly equal to, and above the cusp energy. Our results are compared with recent experimental measurements and other theoretical calculations. The proposed 3$\tilde{\mathrm{C}}$ model yields very encouraging results and paves the way towards a more advanced Lippmann–Schwinger approach based on the 3C model.

Keywords: proton-impact ionization; quasi-Sturmian functions; 3C model; Coulomb three-body Green's function

Check for updates

Academic Editors: Pascal Quinet and Frank B. Rosmej

Received: 17 March 2026
Revised: 17 April 2026
Accepted: 23 April 2026
Published: 26 April 2026

Copyright: © 2026 by the authors. Licensee MDPI, Basel, Switzerland. This article is an open access article distributed under the terms and conditions of the Creative Commons Attribution (CC BY) license.

1. Introduction

Ionization of atoms under the impact of charged heavy particles is a fundamental phenomenon from both theoretical and practical perspectives. The most complete information on the single ionization process, which is a difficult many-body Coulomb problem above the break-up threshold for three free charged particles (incident ion, residual ion, and electron), is provided by the fully differential cross section (FDCS). For ionization of helium by 75 keV proton impact, detailed FDCS measurements have recently become available, e.g., [1–7]. While the results of comparing theoretical predictions with experiment can be considered satisfactory at high incident projectile energies [8,9], at intermediate energies, the situation becomes more complicated. Indeed, as the impact energy decreases, a major theoretical difficulty arises because of the increasing importance of electron capture to the continuum (ECC), to a point that it becomes necessary to consider charge exchange

channels on a par with the direct ionization (DI) mechanism. In order to include explicit allowance for exchange, theoretical approaches based on the use of two-centered bases (one that is centered on the target nucleus and the other accommodated on the projectile), such as the coupled pseudostate (CP) method [10] and the wave-packet convergent close-coupling (WP-CCC) method [11] have been developed. The latter is a sophisticated approach that allows us to obtain, as of today, the most accurate description of the four-body $p^+ + \mathrm{He}$ total scattering wave function. From the corresponding solution components, the DI and ECC amplitudes are extracted by projecting, respectively, onto the continuum states of the (e^-, He^+) and (e^-, p^+) subsystems. However, such an approach leaves ambiguity in determining the ionization cross section, since one can choose a 'coherent' or 'incoherent' combination of the obtained ECC and DI amplitudes; indeed, the components with completely different asymptotic behavior correspond to these two processes.

We have recently developed an approach [9] based on a representation of the final-state three-body wave function in terms of parabolic convoluted quasi-Sturmian (CQS) functions. These basis functions are obtained by applying the Coulomb Green's function for a model three-body Hamiltonian, which can be solved analytically. In order to describe the DI and ECC ionization mechanisms, we have formulated CQS functions for two model Hamiltonians, each of which is separable in its own pair of Jacobi coordinates. In a first model, named 2C [12], the Coulomb Hamiltonian $\hat{H}_2$ is expressed in the pair of coordinates $(\mathbf{r}, \mathbf{R})$, where $\mathbf{r}$ and $\mathbf{R}$ denote, respectively, the position of the electron and the projectile relative to the target; the CQS functions are obtained by applying the corresponding Green's function operator $\hat{G}_2$. In this model, the interactions of the projectile p^+ and the ionized electron with the ionized target He^+ are fully taken into account. In a second model, named IIC [13], one considers a Hamiltonian $\hat{H}_{II}$, expressed in a coordinate set that includes the position vector $\mathbf{r}_{pe} = \mathbf{r} - \mathbf{R}$ of the electron relative to the proton. In this case, one fully takes into account the interactions of the projectile with the ionized target and with the ejected electron, and the CQS basis functions are obtained using the corresponding Green's function operator $\hat{G}_{II}$. It is worth noting that there is a direct analogy between the use of these two types of CQS basis functions and the approach based on the use of two-center bases. Each of the model Hamiltonians $\hat{H}_2$ and $\hat{H}_{II}$ includes its own pair of Coulomb interactions in the three-body system $(e^-, \mathrm{He}^+, p^+)$. In both cases, the remaining (third) Coulomb interaction can be accounted for within the framework of a driven Lippmann–Schwinger (LS) equation; we thus have the 2C+LS and IIC+LS methods. It has been numerically demonstrated, for example, that the 2C + LS method is effective in describing the direct ionization mechanism, which is dominated by the interaction between the ejected electron and the target nucleus. In the velocity matching regime, when it becomes essential to take account of the ECC channel, the IIC approach demonstrates a clear advantage in describing the forward peak [14]. However, due to the long-range nature of Coulomb forces, the ability of these LS equations to convey all the details of the final-state asymptotic behavior is limited; this is manifested in discrepancies between the cross sections calculated in the 2C + LS and IIC + LS approaches and the experimental data. So, in general, it appears that a combination of the results from both of these methods is required to achieve agreement with the experiment.

We now wish to go beyond these two-Jacobi coordinate models and consider an approximate three-body approach to the final-state continuum wave function. To this end, we consider the 3C model function which, as far as we know, was independently derived by Merkur'ev [15] and by Garibotti and Miraglia [16], and later on by Brauner, Briggs and Klar [17], to study, respectively, ion-atom and electron-atom ionization processes within the first Born approximation (more specifically, the first calculations were performed on hydrogen for proton and electron impact). This well-known 3C wave function accounts

for all three Coulomb pair interactions, has a rather simple analytical form, and is designed to exhibit the correct leading-order asymptotic behavior when all three particles are far apart. It is expected to perform best when the relative particle velocities are sufficiently large. From 1990 onwards, many other variants have been proposed to account for short-range effects, including distorted-wave versions and position- or momentum-dependent effective charges. Since it inherently involves important physics and can be readily implemented for numerical calculations, the 3C function has been widely used in many ionization studies, such as double photoionization and single ionization of atomic or molecular targets by particle impact. In the case of the proton-helium ionization process, differential cross-section calculations performed both within the 3C model itself and by approximate approaches based upon it—such as the continuum distorted-wave eikonal initial-state with the interaction between the projectile and the residual-target ion (PT)-included (CDW-EIS-PT) method [5] and the three-body distorted-wave eikonal initial-state (3DW-EIS) approach [4]—show that the model wave function can be considered as a reasonable approximation to the three-body system continuum final state. Indeed, the results for FDCSs obtained within the perturbative approaches [4,5] are in good agreement with those calculated by the ab initio WP-CCC method [18] over a wide range of ejected electron energies. It is worth emphasizing here that the computational resources necessary for carrying out such 3C-type calculations are incomparably more modest than those characteristic of the implementation of the WP-CCC approach. To go beyond the cited 3C approaches, it would be interesting to build an LS method based on the 3C model wave function. This, however, requires the knowledge—which is not available—of the Coulomb three-body Green's function $\hat{G}$. This is why a 3C + LS method has not yet been implemented. The present investigation aims to take a step towards building such an approach.

In this paper, we propose extending the CQS approach by including all three pairwise Coulomb interactions in the construction of the basis functions. Specifically, we suggest using the unknown Coulomb three-body Green's function $\hat{G}$, an ansatz $\hat{\tilde{G}}_3$, obtained by supplying the $\hat{G}_2$ operator with the Coulomb waves appearing in the well-known 3C continuum wave function [16,17]. Instead of extending the basis space with proton-centered functions, we propose, therefore, to adapt the 2C model functions to solve the problem of charge exchange in the continuum; this is achieved by inserting a factor depending on the corresponding parabolic coordinate $\xi_{pe} = r_{pe} + \hat{\mathbf{k}}_{pe} \cdot \mathbf{r}_{pe}$, where $\mathbf{k}_{pe}$ is the relative momentum for the (e^-, p^+) pair. We name this model 3$\tilde{\text{C}}$. The LS-type equation obtained with the proposed ansatz $\hat{\tilde{G}}_3$ can be considered a variant 3$\tilde{\text{C}}$ + LS going beyond the 3C model. Since the 3$\tilde{\text{C}}$ approach considers all three pairwise interactions, solving such an LS equation should provide an unambiguous ionization amplitude that equally accounts for both the DI and ECC mechanisms.

In order to test the functionality of the proposed scheme, we restrict ourselves to the zero-order approximation, i.e., the 3$\tilde{\text{C}}$ model representation. We present here a comparison of calculated FDCS with those obtained within the above theoretical approaches, as well as with those measured experimentally. As we are interested in assessing the effect of accounting for specific Coulomb interactions exactly in the three-body system across various energy regimes, we also compare the 3$\tilde{\text{C}}$ model FDCSs with 2C + LS and IIC calculations.

The remainder of this paper is as follows. We start in Section 2.2, by recalling the 2C model formulation within our CQS approach [13]. Next, based on the model Green's function $\hat{G}_2$, we propose in Section 2.2.2 the ansatz $\hat{\tilde{G}}_3$ for the Coulomb three-body Green's function operator $\hat{G}_3$. Here, we show that the direct application of this approximation is equivalent to using a correlated three-body Coulomb continuum final-state wave function of the 3C model. In turn, the exact solution is cast as a driven equation of the LS-type with a perturbation term represented by the 'off-diagonal part' of the kinetic energy operator [19].

To numerically test the applicability of the extended basis to the solution of the ionization problem, here we limit ourselves to our 3$\tilde{C}$ model. FDCS results are presented in Section 3 for 75 keV proton impact on atomic helium, for electrons ejected into the scattering plane, both in the velocity matching regime and at projectile energy losses well below and above the matching velocity. Specifically, the FDCSs are calculated for relatively large proton-scattering angles, where a noticeable discrepancy between other theoretical predictions and experiment is observed. In this regard, the case of the electron emission into the perpendicular plane, also considered here, is indicative. Finally, we compare our results with calculations reported in the literature. In Section 4, we present our conclusions.

Atomic units (a.u.) in which $\hbar = e = m_e = 1$ are used throughout unless otherwise specified.

2. Theory

We consider a proton of mass m_p incident with momentum $\mathbf{K}_0$ (directed along the z-axis) upon a stationary helium target. In the ionization experiments under consideration, the energy of the ejected electron is determined by the energy loss of the projectile, namely, $E_e = E_{loss} - I$, where $I = 24.59$ eV is the ionization potential of the helium target. The residual He^+ ion is left in the hydrogenic ground state. Further, it is assumed that the target remains at rest during the process. In this approximation, the final state problem is reduced to the motion of two charged particles—a proton and the ejected electron—in the Coulomb field of a stationary force center (a charged body of infinite mass). Let $\mathbf{K}$ and $\mathbf{k}_e$ be the momentum of the proton and electron in the laboratory frame; their total energy $E = \frac{K^2}{2m_p} + \frac{k_e^2}{2}$ is determined by the expression $E = \frac{K_0^2}{2m_p} + \mathcal{E}_{\mathrm{He}} - \mathcal{E}_{\mathrm{He}^+}$, where $\mathcal{E}_{\mathrm{He}} = -2.903724$ a.u. and $\mathcal{E}_{\mathrm{He}^+} = -2$ a.u. The momentum transfer is defined as $\mathbf{q} = \mathbf{K}_0 - \mathbf{K}$.

2.1. General Formulation

Let $\mathbf{R}$ be the position vector of the projectile, while $\mathbf{r}$ and $\mathbf{r}'$ denote the coordinates of the target electrons. The initial state wave function

$$e^{i\mathbf{K}_0\cdot\mathbf{R}}\Phi^{(0)}(\mathbf{r},\mathbf{r}') \tag{1}$$

is expressed as the product of the plane wave $|\mathbf{K}_0\rangle$ for the projectile and the helium ground state wave function $\Phi^{(0)}$. The incident channel interaction is given by

$$V = \frac{2}{R} - \frac{1}{|\mathbf{R}-\mathbf{r}|} - \frac{1}{|\mathbf{R}-\mathbf{r}'|}. \tag{2}$$

We treat the ionization process in the frozen-core approximation for the residual helium ion. Let

$$F(\mathbf{R},\mathbf{r}) = \left\langle \psi_{1s}^{He^+} \middle| \hat{V} \middle| \Phi^{(0)} \right\rangle; \tag{3}$$

the transition amplitude reads

$$T_{\mathbf{K},\mathbf{k}_e} = \left\langle \Psi_{\mathbf{K},\mathbf{k}_e}^{(-)} \middle| \mathbf{K}_0, F \right\rangle, \tag{4}$$

where $\Psi_{\mathbf{K},\mathbf{k}_e}^{(-)}$ is the continuum state of the three-body system $(e^-, \mathrm{He}^+, p^+)$ Hamiltonian

$$\hat{H} = -\frac{1}{2m_p}\nabla_{\mathbf{R}}^2 - \frac{1}{2}\nabla_{\mathbf{r}}^2 + \frac{1}{R} - \frac{1}{r} - \frac{1}{|\mathbf{R}-\mathbf{r}|}. \tag{5}$$

The transition amplitude can also be obtained by taking advantage of the properties of the Green's function operator $\hat{G}^{(+)} \equiv \left[E + i\varepsilon - \hat{H}\right]^{-1}$ [20], namely by solving the driven equation

$$\left[E - \hat{H}\right]\left|\Phi^{(+)}\right\rangle = |\mathbf{K}_0, F\rangle, \tag{6}$$

together with outgoing boundary conditions. The driving term is short-range and determines the behavior of the solution $\Phi^{(+)}$. From its asymptotic behavior for a large hyperradius $\rho = \sqrt{m_p R^2 + r^2}$,

$$\begin{aligned}\left\langle \mathbf{R}, \mathbf{r}\middle|\Phi^{(+)}\right\rangle &= \left\langle \mathbf{R}, \mathbf{r}\middle|\hat{G}^{(+)}\middle|\mathbf{K}_0, F\right\rangle \\ &\simeq \frac{m_p}{(2\pi)^2}\frac{(2E)^{3/4}e^{\frac{i\pi}{4}}}{(2\pi)^{1/2}}\frac{\exp\left\{i\left[\sqrt{2E}\rho + W_0(\mathbf{R}, \mathbf{r})\right]\right\}}{\rho^{5/2}}\left\langle \Psi^{(-)}_{\mathbf{K},\mathbf{k}_e}\middle|\mathbf{K}_0, F\right\rangle,\end{aligned} \tag{7}$$

one can extract the desired amplitude (4) [9]. Here, the $\hat{\mathbf{K}}$ and $\hat{\mathbf{k}}_e$ directions are those of $\hat{\mathbf{R}}$ and $\hat{\mathbf{r}}$, respectively; W_0 is the three-body Coulomb phase [20].

2.2. Parabolic CQS

We propose to solve the driven Equation (6) in parabolic coordinates: $\xi = r + z$, $\eta = r - z$, and $\phi = \tan^{-1}(y/x)$. In the region of the configuration space where the short-range driven term plays a role, we describe the system using square-integrable Sturmians of parabolic coordinates [21,22]:

$$\langle \xi, \eta, \phi\,|n, m, \varkappa\rangle = \frac{e^{i\varkappa\phi}}{\sqrt{2\pi}}\,\varphi_n^{|\varkappa|}(\xi)\,\varphi_m^{|\varkappa|}(\eta), \tag{8}$$

where

$$\varphi_n^{\lambda}(\rho) = \sqrt{\frac{2bn!}{(n+\lambda)!}}\,(2b\rho)^{\lambda/2}e^{-b\rho}L_n^{\lambda}(2b\rho), \quad \lambda = |\varkappa|, \tag{9}$$

with the basis scale parameter b. Along with the basis functions (8), we also define their orthogonal complements

$$|\widetilde{n, m, \varkappa}\rangle = w|n, m, \varkappa\rangle, \quad w(\xi, \eta) = \frac{4}{\xi + \eta} \tag{10}$$

such that

$$\langle\widetilde{n, m, \varkappa}|n', m', \varkappa'\rangle = \delta_{nn'}\delta_{mm'}\delta_{\varkappa\varkappa'}. \tag{11}$$

Furthermore, let $\left|Q; \widetilde{n, m, \varkappa}\right\rangle$ denote the orthogonal complement (10), equipped with a phase factor

$$\langle \mathbf{r}\,|Q\rangle = e^{iQz}. \tag{12}$$

Consider a Coulomb wave, for a Sommerfeld parameter β and a momentum $\mathbf{P}$ with polar angles (θ, φ),

$$\Psi^{(-)}_{\mathbf{P}}(\beta, \mathbf{r}) = e^{-\frac{\pi\beta}{2}}\Gamma(1 - i\beta)e^{i\mathbf{P}\cdot\mathbf{r}}\mathcal{M}(i\beta, 1; -i[Pr + \mathbf{P}\cdot\mathbf{r}]), \tag{13}$$

where $\mathcal{M}$ is a Kummer function [23]. We shall see below that, in the 2C and 3$\tilde{\text{C}}$ models, the ionization amplitude (4) can be expressed in terms of so-called basis amplitudes $\mathcal{A}^{(+)}_{n,m,\lambda}$ defined through the projection

$$\left\langle \Psi^{(-)}_{\mathbf{P}}(\beta)\middle|Q; \widetilde{n, m, \varkappa}\right\rangle = \sqrt{2\pi}e^{i\varkappa\phi}\mathcal{A}^{(+)}_{n,m,\lambda}(\beta, P, Q;\ \theta), \quad \lambda = |\varkappa|. \tag{14}$$

It turns out that they offer the advantage of being expressed in closed form [9]

$$\begin{aligned}\mathcal{A}^{(+)}_{n,m,\lambda}(\beta,P,Q;\,\theta) &= \tfrac{i}{P}\sqrt{\tfrac{n!m!}{(n+\lambda)!(m+\lambda)!}}\left[\tfrac{1+(p+q)}{1-(p-q)}\tfrac{1}{c^2+\alpha s^2}\right]^{i\beta}e^{-\frac{\pi\beta}{2}}\\ &\times\left[\tfrac{4p}{1-(p-q)^2}\tfrac{1}{c^2+\alpha s^2}\right]^{1+\lambda}\left(\tfrac{\sin\theta}{2}\right)^{\lambda}\left[-\tfrac{1-(p+q)}{1+(p+q)}\right]^{n}\left[-\tfrac{1-(p-q)}{1+(p-q)}\right]^{m}\\ &\times\sum_{\nu=0}^{n}\sum_{\mu=0}^{m}c_{\nu}^{(n,\lambda)}c_{\mu}^{(m,\lambda)}\,\Gamma(i\beta+\lambda+\nu+\mu+1)\\ &\times\left[\tfrac{-4p}{[1-(p+q)][1-(p-q)]}\tfrac{1}{c^2+\alpha s^2}\right]^{\nu+\mu}(c^2)^{\nu}(\alpha s^2)^{\mu},\end{aligned}\tag{15}$$

where

$$p=-\tfrac{iP}{2b},\quad q=-\tfrac{iQ}{2b},\quad \alpha=\tfrac{1-(p+q)^2}{1-(p-q)^2},\qquad c=\cos\tfrac{\theta}{2},\quad s=\sin\tfrac{\theta}{2},\tag{16}$$

$$c_{\nu}^{(n,\lambda)}=(-1)^{\nu}\frac{(n+\lambda)!}{(n-\nu)!(\nu+\lambda)!\nu!}.\tag{17}$$

2.2.1. 2C and 2C + LS Models

Within the 2C model, one considers the Jacobi coordinate pair $(\mathbf{R},\mathbf{r})$ and the separable Hamiltonian

$$\hat{H}_2=-\frac{1}{2m_p}\nabla^2_{\mathbf{R}}-\frac{1}{2}\nabla^2_{\mathbf{r}}+\frac{1}{R}-\frac{1}{r}.\tag{18}$$

The continuum solution is the product $\left|\Psi^{(-)}_{\mathbf{K}},\Psi^{(-)}_{\mathbf{k}_e}\right\rangle$, where $\Psi^{(-)}_{\mathbf{K}}(\beta_p=\frac{m_p}{K})$ and $\Psi^{(-)}_{\mathbf{k}_e}$ $(\beta_e=-\frac{1}{k_e})$ denote the proton and electron Coulomb waves (13), respectively. The simplified Hamiltonian $\hat{H}_2$ also implies that the operator $\hat{G}^{(+)}$ of the Coulomb three-body Green's function is approximated by $\hat{G}^{(+)}_2=\left[E+\mathrm{i}\varepsilon-\hat{H}_2\right]^{-1}$. The amplitude of the 2C model reads

$$T^{(2C)}_{\mathbf{K},\mathbf{k}_e}=\sqrt{2}\left\langle\Psi^{(-)}_{\mathbf{K}},\Psi^{(-)}_{\mathbf{k}_e}\middle|\mathbf{K}_0,F\right\rangle,\tag{19}$$

where the factor $\sqrt{2}$ is related to the fact that there are two identical target electrons. Here, we neglect the exchange between the active electron and the core electron.

Let $\xi_{\mathbf{R}}$, $\eta_{\mathbf{R}}$, $\phi_{\mathbf{R}}$ and $\xi_{\mathbf{r}}$, $\eta_{\mathbf{r}}$, $\phi_{\mathbf{r}}$ be sets of parabolic coordinates associated with $\mathbf{R}$ and $\mathbf{r}$, respectively. We denote the corresponding Sturmians as $|\mathfrak{n}\rangle_{\mathbf{R}}$ and $|\mathfrak{m}\rangle_{\mathbf{r}}$:

$$|\mathfrak{n}\rangle_{\mathbf{R}}\equiv|n_1,n_2,\varkappa\rangle_{\mathbf{R}}\quad,\quad|\mathfrak{m}\rangle_{\mathbf{r}}\equiv|m_1,m_2,-\varkappa\rangle_{\mathbf{r}}.\tag{20}$$

Note that the state of the three-body system is characterized by a zero total magnetic quantum number. We expand the driven term of Equation (6) into products $|K_0;\mathfrak{n}\rangle_{\mathbf{R}}|\mathfrak{m}\rangle_{\mathbf{r}}$ and apply the Green's function operator $\hat{G}^{(+)}_2$ to the orthogonal complements $|K_0;\widetilde{\mathfrak{n}}\rangle_{\mathbf{R}}|\widetilde{\mathfrak{m}}\rangle_{\mathbf{r}}$. Taking into account the projection expression (14), one obtains for the 2C ionization amplitude [13]:

$$T^{(2C)}_{\mathbf{K},\mathbf{k}_e}=2\pi\sqrt{2}\sum_{\mathfrak{n},\mathfrak{m}}C^{(2C)}_{\mathfrak{n},\mathfrak{m}}e^{i\varkappa(\phi_p-\phi_e)}\mathcal{A}^{(+)}_{\mathfrak{n}}(\beta_p,K,K_0;\,\theta_p)\,\mathcal{A}^{(+)}_{\mathfrak{m}}(\beta_e,k_e,0;\,\theta_e),\tag{21}$$

where the coefficients $C^{(2C)}_{\mathfrak{n},\mathfrak{m}}$ are defined by

$$C^{(2C)}_{\mathfrak{n},\mathfrak{m}}\equiv\{{}_{\mathbf{R}}\langle\mathfrak{n}|\,{}_{\mathbf{r}}\langle\mathfrak{m}|\,\}F\rangle.\tag{22}$$

In order to go beyond the 2C model, it has been proposed [13] to expand the solution $\left|\Phi^{(+)}\right\rangle$ of the driven Equation (6) on the CQS basis functions $\left|\mathcal{S}^{(2)}_{\mathfrak{n},\mathfrak{m}}\right\rangle$ determined by applying the Green's function operator $\hat{G}_2^{(+)}$ to the orthogonal complements:

$$\left|\mathcal{S}^{(2)}_{\mathfrak{n},\mathfrak{m}}\right\rangle = \hat{G}_2^{(+)}|K_0,\widetilde{\mathfrak{n}}\rangle_{\mathbf{R}}|\widetilde{\mathfrak{m}}\rangle_{\mathbf{r}}. \tag{23}$$

Inserting the expansion

$$\left|\Phi^{(+)}\right\rangle = \sum_{\mathfrak{n},\mathfrak{m}} C^{(2)}_{\mathfrak{n},\mathfrak{m}}\left|\mathcal{S}^{(2)}_{\mathfrak{n},\mathfrak{m}}\right\rangle \tag{24}$$

into (6) yields a LS-type equation for the coefficients $C^{(2)}_{\mathfrak{n},\mathfrak{m}}$:

$$\sum_{\mathfrak{n},\mathfrak{m}}\left[\hat{I}-\hat{U}\hat{G}_2^{(+)}\right]C^{(2)}_{\mathfrak{n},\mathfrak{m}}|K_0,\widetilde{\mathfrak{n}}\rangle_{\mathbf{R}}|\widetilde{\mathfrak{m}}\rangle_{\mathbf{r}} = |\mathbf{K}_0,F\rangle, \tag{25}$$

where $\hat{U}$ denotes the proton–electron potential

$$\hat{U} = -\frac{1}{|\mathbf{R}-\mathbf{r}|}. \tag{26}$$

Multiplying this equation by $\{{}_{\mathbf{R}}\langle\mathbf{K}_0;\mathfrak{n}'|\,{}_{\mathbf{r}}\langle\mathfrak{m}'|\}$, we obtain a matrix equation which can be solved with standard techniques [9]. Once the coefficients $C^{(2)}_{\mathfrak{n},\mathfrak{m}}$ are found, one gets the 2C+LS ionization amplitude $T^{(2C+LS)}_{\mathbf{K},\mathbf{k}_e}$.

2.2.2. 3$\tilde{C}$ Model

We now wish to improve the approach by including in the 2C model some features of the well-known 3C model [15–17]. On top of the product of two Coulomb functions, the 3C wave function has a multiplicative Kummer function related to the third Coulomb interaction, the proton–electron interaction in our case. Within what we shall name the 3$\tilde{C}$ model, we consider the relative coordinate $\mathbf{r}_{pe} = \mathbf{r}-\mathbf{R}$ and introduce the associated parabolic coordinate

$$\xi_{pe} \equiv r_{pe} + \hat{\mathbf{k}}_{pe}\cdot\mathbf{r}_{pe}, \tag{27}$$

where the momentum

$$\mathbf{k}_{pe} = \frac{m_p}{m_p+1}\mathbf{k}_e - \frac{1}{m_p+1}\mathbf{K} \tag{28}$$

is conjugate to the coordinate $\mathbf{r}_{pe}$. In order to take into account the proton–electron interaction in a way similar to the 3C model, we propose an approximate three-body Green's function operator $\hat{\tilde{G}}_3^{(+)}$ by modifying the Green's function of the 2C model as follows:

$$\hat{\tilde{G}}_3^{(+)} = |\mathcal{U}\rangle\hat{G}_2^{(+)}\langle\mathcal{F}|, \tag{29}$$

where

$$\langle\xi_{pe}|\mathcal{F}\rangle = \Gamma(1-i\beta_{pe})\mathcal{M}(i\beta_{pe},1;-ik_{pe}\xi_{pe}), \tag{30}$$

$$\langle\xi_{pe}|\mathcal{U}\rangle = \mathcal{U}(i\beta_{pe},1;-ik_{pe}\xi_{pe}), \tag{31}$$

with the Sommerfeld parameter $\beta_{pe} = -\frac{m_p}{(m_p+1)}\frac{1}{k_{pe}}$. Using the leading asymptotic behaviors of the Kummer functions $\mathcal{U}$ and $\mathcal{M}$ [23], we deduce the asymptotic behavior of $\hat{\tilde{G}}_3$ for large ρ

$$\left\langle \mathbf{R},\mathbf{r}\middle|\hat{\tilde{G}}_3^{(+)}\middle|\mathbf{K}_0,F\right\rangle \simeq \frac{m_p}{(2\pi)^2}\frac{(2E)^{3/4}e^{\frac{i\pi}{4}}}{(2\pi)^{1/2}}\frac{\exp\left\{i\left[\sqrt{2E}\rho-\beta_p\ln(2KR)-\beta_e\ln(2k_er)-\beta_{pe}\ln(k_{pe}\xi_{pe})\right]\right\}}{\rho^{5/2}} \times e^{-\frac{\pi\beta_{pe}}{2}}\left\langle \Psi_{\mathbf{K}}^{(-)}(\beta_p),\Psi_{\mathbf{k}_e}^{(-)}(\beta_e),\mathcal{F}\middle|\mathbf{K}_0,F\right\rangle. \tag{32}$$

By comparing (32) with the asymptotic behavior (7) of the true Green's function, we find that the 3$\tilde{\text{C}}$ model amplitude (up to a phase factor) can be represented as

$$T_{\mathbf{K},\mathbf{k}_e}^{(3\tilde{\text{C}})}=\sqrt{2}\,e^{-\frac{\pi\beta_{pe}}{2}}\left\langle \Psi_{\mathbf{K}}^{(-)},\Psi_{\mathbf{k}_e}^{(-)},\mathcal{F}\middle|\mathbf{K}_0,F\right\rangle, \tag{33}$$

which strongly resembles the 3C model amplitude [16,17]. To calculate it, we use the expansion

$$\left|\mathcal{F}\right\rangle=\sum_{\ell=0}^{\infty}s_\ell(k_{pe})|\ell\rangle, \tag{34}$$

in terms of basis L^2 functions:

$$\langle\xi_{pe}|\ell\,\rangle=\sqrt{2b}e^{-b\xi_{pe}}L_\ell(2b\xi_{pe}). \tag{35}$$

The coefficients in (34) are analytically given by

$$s_\ell(k_{pe})=s_0(k_{pe})p_\ell(k_{pe}), \tag{36}$$

where

$$s_0(k_{pe})=\Gamma(1-i\beta_{pe})\sqrt{\frac{2}{b}}\left(1+i\frac{k_{pe}}{b}\right)^{-i\beta_{pe}}, \tag{37}$$

$$p_\ell(k_{pe})=(-1)^\ell{}_2F_1(-\ell,i\beta_{pe};1;1-\zeta),\quad \zeta=\frac{b-ik_{pe}}{b+ik_{pe}}. \tag{38}$$

Finally, we obtain the following representation of the amplitude (33) in the 3$\tilde{\text{C}}$ model:

$$T_{\mathbf{K},\mathbf{k}_e}^{(3\tilde{\text{C}})}=2\pi\sqrt{2}\,e^{-\frac{\pi\beta_{pe}}{2}}\sum_{\mathfrak{n},\mathfrak{m},\ell}C_{\mathfrak{n},\mathfrak{m},\ell}^{(3\tilde{\text{C}})}e^{i\varkappa(\phi_p-\phi_e)}\mathcal{A}_{\mathfrak{n}}^{(+)}(\beta_p,K,K_0;\,\theta_p)\,\mathcal{A}_{\mathfrak{m}}^{(+)}(\beta_e,k_e,0;\,\theta_e)s_\ell^*(k_{pe}), \tag{39}$$

where the coefficients

$$C_{\mathfrak{n},\mathfrak{m},\ell}^{(3\tilde{\text{C}})}=\{\,{}_{\mathbf{R}}\langle\mathfrak{n}|\;{}_{\mathbf{r}}\langle\mathfrak{m}|_{pe}\langle\ell|\,\}F\rangle \tag{40}$$

are six-dimensional integrals whose integrands feature exponentials and Laguerre polynomials. With the parabolic coordinate ξ_{pe} being defined by (27), the coefficients $C_{\mathfrak{n},\mathfrak{m},\ell}^{(3\tilde{\text{C}})}$ carry the dependence on the momenta $\mathbf{K}$ and $\mathbf{k}_e$.

To go beyond the 3$\tilde{\text{C}}$ model, we may proceed similarly to the 2C model, through an LS-type equation. To this end, we propose an improved approximation of the solution of the driven Equation (6) through an expansion

$$\left|\Phi^{(+)}\right\rangle=\sum_{\mathfrak{n},\mathfrak{m},\ell}C_{\mathfrak{n},\mathfrak{m},\ell}^{(3)}\left|\mathcal{S}_{\mathfrak{n},\mathfrak{m},\ell}^{(3)}\right\rangle, \tag{41}$$

in the space of quasi-Sturmian functions defined by

$$\left|\mathcal{S}_{\mathfrak{n},\mathfrak{m},\ell}^{(3)}\right\rangle=\hat{\tilde{G}}_3^{(+)}|K_0;\widetilde{\mathfrak{n}}\rangle_{\mathbf{R}}|\widetilde{\mathfrak{m}}\rangle_{\mathbf{r}}|\ell\rangle_{pe}. \tag{42}$$

Specifically, inserting such an expansion into Equation (6) gives the following LS-type equation:

$$\sum_{\mathfrak{n},\mathfrak{m},\ell}\Big[|\mathcal{U}\rangle+\Big|\frac{\partial}{\partial\xi_{pe}}\mathcal{U}\Big\rangle\Big\{\Big(\frac{\mathbf{r}_{pe}}{r_{pe}}+\frac{\mathbf{k}_{pe}}{k_{pe}}\Big)\cdot\Big(\nabla_{\mathbf{r}}\hat{G}_2^{(+)}-\frac{1}{m_p}\nabla_{\mathbf{R}}\hat{G}_2^{(+)}\Big)$$
$$-\frac{(m_p+1)}{m_p}\frac{ik_{pe}\xi_{pe}}{r_{pe}}\hat{G}_2^{(+)}\Big\}\Big]\,C^{(3)}_{\mathfrak{n},\mathfrak{m},\ell}\langle\mathcal{F}\{|K_0,\widetilde{\mathfrak{n}}\rangle_{\mathbf{R}}|\widetilde{\mathfrak{m}}\rangle_{\mathbf{r}}|\ell\rangle_{pe}\}=\Big|\mathbf{K}_0,F\Big\rangle. \tag{43}$$

By projection, one obtains a matrix equation whose solutions provide the coefficients $C^{(3)}_{\mathfrak{n},\mathfrak{m},\ell}$, which in turn build the 3$\tilde{C}$+LS ionization amplitude $T^{(3\tilde{C}+LS)}_{\mathbf{K},\mathbf{k}_e}$. Here it is worth noting that the LS-type Equation (43) differs considerably from that given by Equation (25) since the proton–electron Coulomb interaction $\hat{U}$ is replaced by a term produced by the action of the kinetic energy operator on the basis CQS functions (42). Thus, at the operator level, the proposed approach could be considered as a complete account of all pairwise Coulomb interactions. We believe that the LS Equation (43) will ensure the elimination of the approximations made in the formulation of the ansatz of the Coulomb three-body Green's function, which, as we have seen, are also characteristic of the 3C model.

3. Results and Discussion

With the ionization amplitudes $T^{(2C)}_{\mathbf{K},\mathbf{k}_e}$, $T^{(2C+LS)}_{\mathbf{K},\mathbf{k}_e}$, or $T^{(3\tilde{C})}_{\mathbf{K},\mathbf{k}_e}$, we have calculated the FDCSs in the laboratory frame:

$$\frac{d^5\sigma}{dE_e d\Omega_e d\Omega_p}=k_e\frac{m_p^2}{(2\pi)^5}\frac{K}{K_0}|T_{\mathbf{K},\mathbf{k}_e}|^2 \tag{44}$$

for ionization of helium by 75 keV proton impact under conditions selected in recent experiments [3,4,7,18]. Specifically, the angular distribution of electrons ejected into the scattering plane is investigated at projectile energy losses $E_{loss}=25.6$, 65.5, and 85 eV and for the scattering angle $\theta_p=0.5$ mrad. Thus, in the considered energy regimes, the velocities of the ejected electrons are respectively less than, nearly equal to, and greater than the projectile velocity. In addition, the FDCSs are calculated for a proton energy loss of 30 eV for electrons emitted both in the scattering and perpendicular planes and for the transverse momentum transfer $q_\perp=1.38$ a.u. (i.e., for $\theta_p=0.43$ mrad).

The calculations were made using a quite accurate ground-state wave function $\Phi^{(0)}(\mathbf{r},\mathbf{r}')$ obtained by diagonalizing the helium Hamiltonian matrix representation in the complete square-integrable Laguerre basis set as described in Ref. [24]; the corresponding energy $E_0^{He}=-2.9035$ a.u. ($E_0^{He}=-79.00825304$ eV) is quite close to the experimental or reference value -2.903724 a.u.

Numerically, we found that by choosing the value 1 for the basic scaling parameter b (which was found to be optimal for representing the function $|F\rangle$ in the Sturmian basis (20)), the convergence of expansions (21) and (39) is achieved upon reaching the upper limit of summation determined by the values $M=3$ (i.e., $|\varkappa|\le M$) and $N\simeq 15$. More precisely, the condition $n<N$ applies only to the indices n_1 and n_2 of the 'proton' basis functions $|\mathfrak{n}\rangle_{\mathbf{R}}$ (20), as well as to the index ℓ (in (39)). In turn, the presence of the bound state wave function $\Phi^{(0)}$ of the helium atom leads to a rather rapid decrease in the expansion coefficients $C^{(2C)}_{\mathfrak{n},\mathfrak{m}}$ (22) and $C^{(3\tilde{C})}_{\mathfrak{n},\mathfrak{m},\ell}$ (40) as the indices m_1 and m_2 of the 'electron' basis functions $|\mathfrak{m}\rangle_{\mathbf{r}}$ (20) increase. In particular, it turned out to be sufficient to set $m_j<7$, $j=1,2$ in the summations (21) and (39). It is worth noting that the obtained upper limits of the summations determine the minimum sizes of the basis sets in which the solution of the LS Equation (25) is sought (and it is assumed that the solution (43) will be sought in the future).

At small energy losses, the DI mechanism is dominant [12,18], so one would expect the 2C model to be able to describe all the features of the ionization process. However, as shown in Figure 1, for $E_{loss} = 25.6$ eV, there is significant disagreement between theory and the measured data in both shape and magnitude. In particular, the cross-section obtained within the 2C model completely fails to reproduce the experimentally observed peak at negative ejection angles, which may be identified as the recoil peak. By taking into account the proton–electron interaction within the LS Equation (25), the same failure was surprisingly observed in [12] in which $N = 9$. To further investigate why this feature of the angular distribution could not be found, we have performed the 2C + LS calculation again with a basis set extended by increasing the number of proton basis functions (20), as described above. The resulting FDCS, presented in Figure 1, now features the presence of both a binary peak at $\theta_e = 48^\circ$ and a recoil peak at $\theta_e = -54^\circ$, which is consistent with both the experimental data [7] and the WP-CCC (both one- and two-center) calculations [18].

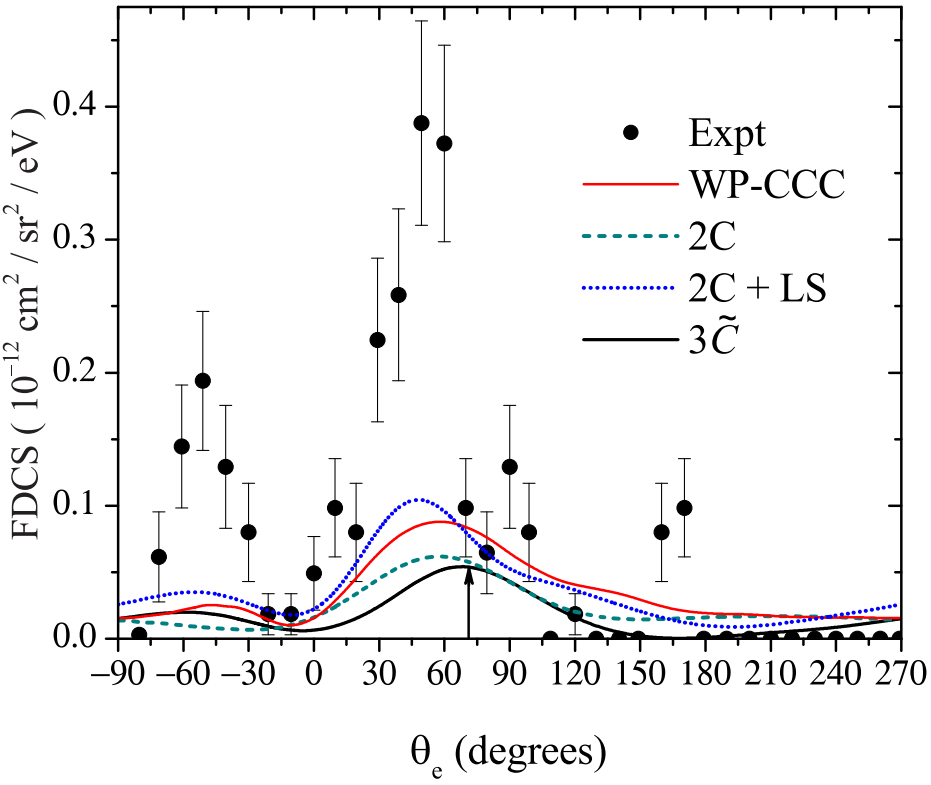


Figure 1. FDCSs for the energy loss of $E_{loss} = 25.6$ eV and the proton scattering angle of $\theta_p = 0.5$ mrad. The 2C model results—dashed line (dark cyan); the 2C + LS model results—dotted line (blue); our 3$\tilde{C}$ model results—thick solid line (black); the WP-CCC results [18]—thin solid line (red). Experiment: solid circles with error bars from Ref. [7]. The arrow indicates the direction of the momentum transfer **q**.

It is also worth noting that the new 2C + LS calculations moved the binary peak in the forward direction significantly relative to the momentum transfer **q**, and thus aligned very well with the experimental observation. The ratio of the binary and the recoil peaks magnitudes is approximately 2.8, while experimentally it is about 2. The FDCS calculated in our 3$\tilde{C}$ model also features a clear two-peak structure. While the absolute magnitude is decreased with respect to the 2C + LS result, the recoil peak is approximately half that of the binary peak, which is consistent with the measurement [7]. However, the angular position of the binary peak is in the **q** direction, and thus differs considerably from the experimental observation. This may be due to the importance of the contribution to the

amplitude, at low electron energies, from a region of space where the 3C approximation of the wave function is no longer applicable.

Qualitatively, the situation does not change fundamentally, with a slight increase in energy losses, which is confirmed by the behavior of the FDCSs for the energy loss of 30 eV and the projectile scattering angle $\theta_p = 0.43$ mrad shown in the left panel of Figure 2. Here, the DI ionization mechanism still dominates, while the ECC contribution is negligible [18]. Once again, the 2C + LS cross section shows a very satisfactory angular distribution, in particular with respect to the binary peak position; it also shows quite acceptable peak magnitudes. In the 3$\tilde{C}$ model, on the other hand, the binary peak is predicted exactly in the **q** direction, similarly to the case described in Figure 1. As can be seen in the right panel of Figure 2, this feature is observed also in several other theoretical approaches; one exception is given by the CDW-EIS result with a binary peak position as the one predicted by the 2C + LS model (note, however, that the CDW-EIS completely fails to predict a recoil peak).

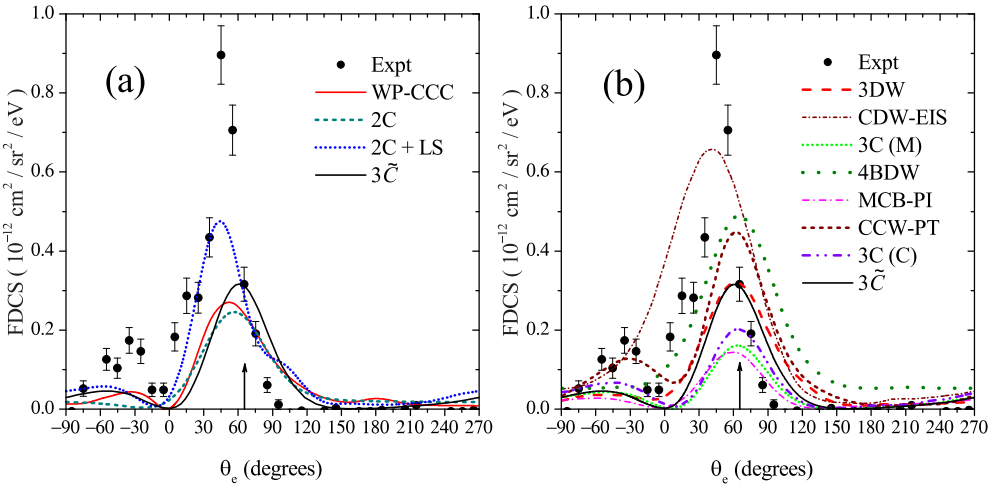


Figure 2. FDCSs for the energy loss of $E_{loss} = 30$ eV and the proton scattering angle of $\theta_p = 0.43$ mrad ($q_\perp = 1.38$ a.u.). Experiment: solid circles with error bars from Ref. [3], corrected in Ref. [18]. In the left panel (**a**): the 2C model results—dashed line (dark cyan); the 2C + LS model results—dotted line (blue); our 3$\tilde{C}$ model results—thick solid line (black); the WP-CCC results [18]—thin solid line (red). In the right panel (**b**): the 3DW results [3]—dashed line (red); the CDW-EIS results [25]—dash dotted line (wine); the 3C (M) results [26]—short dotted line (green); the 4BDW results [27]—dotted line (olive); the MCB-PI results [28]—dash dotted line (magenta); the CCW-PT results [29]—short dotted line (wine); the WP-CCC results [18]—thin solid line (red); the 3C (C) results [30]—dash dot dotted line (violet); our 3$\tilde{C}$ model results—thick solid line (black).

Next, we consider the case of electron emission in the perpendicular plane with the same kinematics. As can be seen from Figure 3, the situation theory-experiment is not satisfactory. Nevertheless, we note that, with all their shortcomings, only the 3C model [26,30] and its variations, including CCW-PT [29] and our 3$\tilde{C}$, are able to at least reproduce the experimentally observed minimum in the FDCS at $\theta_e = 0°$. When assessing the agreement between theoretical predictions and experimental data (panel (b)), various criteria can be used. For example, if the assessment is based on the absolute values of the calculated cross sections relative to the measured ones, then preference should be given to the CCW-PT [29] and CDW-EIS [25] methods; their angular distributions, however, differ substantially, with the CDW-EIS failing to feature a minimum at $\theta_e = 0°$. On the other hand, if the reproduction of the cross-section shape is the primary focus, then the 3C-type models catch that particular feature, though approximately, but fail on the absolute cross-section scale. Panel (a) of Figure 3 clearly demonstrates that this minimum is not present within

the 2C or 2C + LS approach, and that a 3C approach is necessary. As far as we know, no WP-CCC data are available for comparison in this geometry.

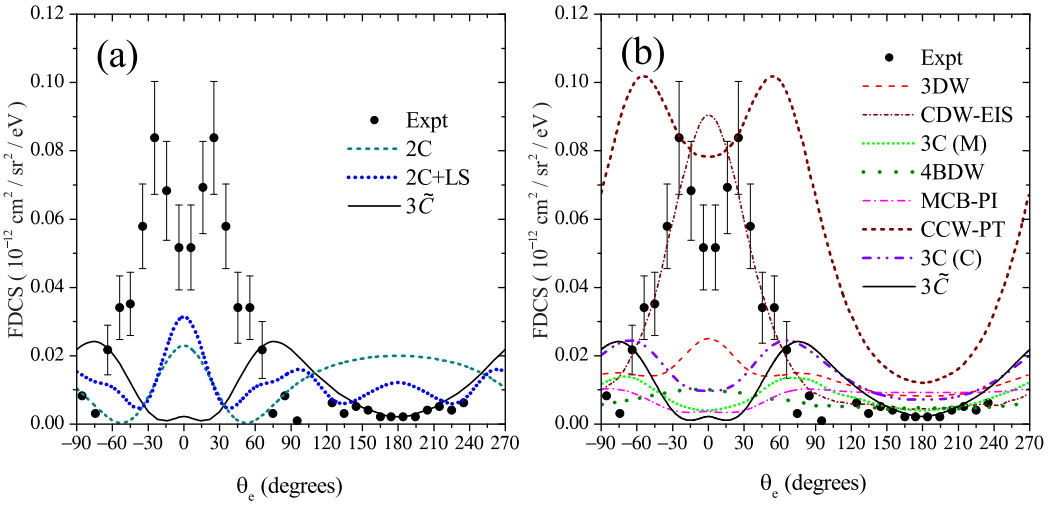


Figure 3. FDCSs for the energy loss of $E_{loss} = 30$ eV and the proton scattering angle of $\theta_p = 0.43$ mrad ($q_\perp = 1.38$ a.u.). The electrons are ejected into the perpendicular plane. Experiment: solid circles with error bars from Ref. [3]. In the left panel (**a**): the 2C model results—dashed line (dark cyan); the 2C + LS model results—dotted line (blue); our 3$\tilde{C}$ model results—thick solid line (black); the WP-CCC results [18]—thin solid line (red). In the right panel (**b**): the 3DW results [3]—dashed line (red); the CDW-EIS results [25]—dash dotted line (wine); the 3C (M) results [26]—short dotted line (green); the 4BDW results [27]—dotted line (olive); the MCB-PI results [28]—dash dotted line (magenta); the CCW-PT results [29]—short dotted line (wine); the WP-CCC results [18]—thin solid line (red); the 3C (C) results [30]—dash dot dotted line (violet); our 3$\tilde{C}$ model results—thick solid line (black).

In the energy regime, when the electron is ejected with a velocity nearly equal to the velocity of the proton (velocity matching), a pronounced peak structure of the experimental angular distribution in the initial projectile beam direction (forward peak) is observed. The presence of this sharp forward peak is explained by the ionization mechanism, which is referred to as electron capture to the continuum. In Figure 4, FDCSs are shown for $E_{loss} = 65.5$ eV. Note that the energy of the ejected electron is now an order of magnitude higher than the value in the cases considered in the previous figures, so that changes in the quality of the 3C model approximation can be expected. From the left panel, we clearly see that our previous 2C + LS calculations [13], as expected, can only describe the binary peak, whereas the IIC model reproduces the forward peak while greatly underestimating the height of the binary peak. Compared to the IIC model, the 3$\tilde{C}$ model yields a narrower forward peak, broadens the binary peak, and increases its magnitude. At the same time, the growth is accompanied by a shift of the binary peak in the forward direction relative to **q** in better agreement with experimental observations. It thus seems that, in this energy regime, the 3$\tilde{C}$ model manages to include the good features of both the 2C and IIC approaches and to produce FDCS results comparable to those measured in the experiment [4]. A favorable comparison with other theoretical approaches is also seen (right panel).

As was found in the experiment [7] at large E_{loss} (above the velocity matching), a residue of the forward peak remains, at least for large θ_p values. For example, in the angular distribution measured at $\theta_p = 0.5$ mrad for $E_{loss} = 85$ eV shown in Figure 5, the well-separated forward peak and binary peak are clearly visible.

Similarly to what was observed in Figure 4, the FDCS obtained within the 2C + LS model features only a strong binary peak and a very weak recoil peak, while the IIC model presents a binary and a clear forward peak, albeit of much reduced magnitude. The forward

peak can still be seen in the FDCS obtained with the 3$\tilde{C}$ model, whereas the WP-CCC model only shows a shoulder. As in the previous case, for the 3$\tilde{C}$ model, there is a clear shift of the binary peak in the forward direction, which is quite expected given that the proton and electron velocities are still close to each other. Thus, the analogy with the previous case also extends to the appropriate behavior of the binary peak (its size and angular position) when moving from the 2C to the 3$\tilde{C}$ model. From the right panel, we observe that the height of the 3$\tilde{C}$ model binary peak is in satisfactory agreement with those obtained with the 3DW-EIS and CDW-EIS-PT models; note that these two model calculations only present a barely visible shoulder in the forward direction.

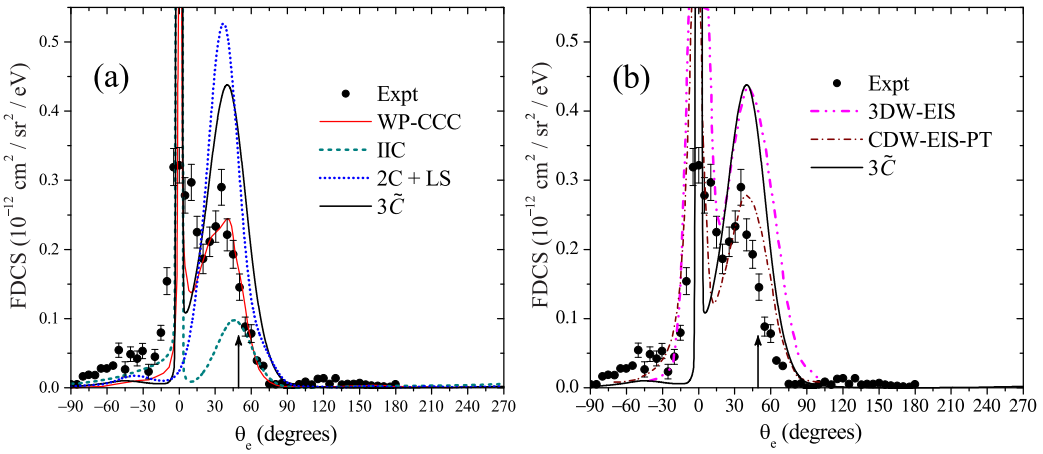


Figure 4. FDCSs for the energy loss of E_{loss} = 65.5 eV and the proton-scattering angle of $\theta_p = 0.5$ mrad. Experiment: solid circles with error bars from Ref. [4]. In the left panel (**a**): the 2C + LS model results—dotted line (blue); the 3$\tilde{C}$ model results—thick solid line (black); the IIC model results—dashed line (dark cyan); the WP-CCC results [18]—thin solid line (red). In the right panel (**b**): the 3DW-EIS results [4]—dashed dot dot line (magenta); the CDW-EIS-PT results [4]—dashed dot line (wine); our 3$\tilde{C}$ model results—thick solid line (black).

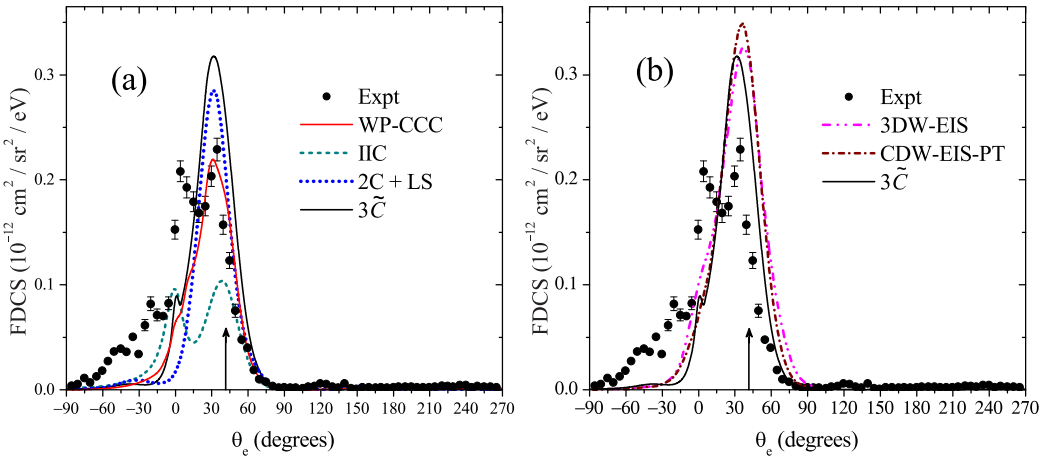


Figure 5. FDCSs for the energy loss of E_{loss} = 85 eV and the proton-scattering angle of $\theta_p = 0.5$ mrad. In the left panel (**a**): the 2C + LS model results—dotted line (blue); the 3$\tilde{C}$ model results—thick solid line (black); the IIC model results—dashed line (dark cyan); the WP-CCC results [18]—thin solid line (red). In the right panel (**b**): the 3DW-EIS results [4]—dashed dot dot line (magenta); the CDW-EIS-PT results [4]—dashed dot line (wine); our 3$\tilde{C}$ model results—thick solid line (black). Experiment: solid circles with error bars from Ref. [7].

From the comparisons presented above, we can conclude that the parabolic CQS implementation of the 3$\tilde{C}$ model, that partially accounts for the three two-particle Coulomb interactions, is applicable to the ionization problem in the energy regime where the contri-

bution of the ECC mechanism is significant. While some specific experimental features are not reproduced, the overall agreement is very encouraging.

4. Summary

This paper is dedicated to the description of the final state continuum wave function of the three-body Coulomb system $(e^-, \mathrm{He}^+, p^+)$, with an application to helium differential ionization at intermediate proton impact energies. We have further developed our CQS approach by somehow considering all three pairwise interactions simultaneously. To this end, we have introduced an ansatz of the Coulomb three-body Green's function. The explicit dependence of the operator on all three relative coordinates of the particles is then imparted to the resulting CQS functions, which can then deal with the situation when the ejected electron is equally affected by both the target and the proton. Thus, an unambiguous ionization amplitude that equally accounts for both the DI and ECC mechanisms can, in principle, be obtained by solving the corresponding Lippmann–Schwinger equation in the representation of these basis functions.

We have evaluated the functionality of the proposed approach by limiting ourselves, in a first step, to using the $3\tilde{C}$ model. We have shown calculations of the FDCSs for proton-impact ionization of atomic helium at 75 keV in various kinematic regimes. Here we would like to highlight the fact that, like other 3C-type calculations, the proposed $3\tilde{C}$ calculations require incomparably fewer computational resources than a non-perturbative approach such as WP-CCC.

In general, the calculations demonstrate an increase in the predictive ability of the $3\tilde{C}$ model for the data under consideration as the energy of the ejected electrons increases. In particular, at low energy losses, when the interaction between the ejected electron and the target nucleus predominates, it is preferable to use the 2C + LS approach, which allows one to correctly describe the angular position of the binary peak. In contrast, in the two-peak structure of cross sections obtained using the $3\tilde{C}$ model, the binary peak is located strictly in the momentum transfer $\mathbf{q}$ direction. At the same time, the 3C model and its variations, including our $3\tilde{C}$, are able to describe the shape of the FDCS and, in particular, to reproduce the minimum at $\theta_e = 0^\circ$ observed in the experiment in the case of electron emission into the perpendicular plane.

At large energy losses reaching the matching velocity and above, the 2C + LS approach is clearly inferior to the $3\tilde{C}$ model. It is sufficient to note here that the 2C + LS approach is, in principle, not capable of reproducing the peak in the forward direction. On the other hand, FDCSs obtained within the IIC model exhibit both a forward peak and a binary peak; however, compared with the measured data, the binary peak height is underestimated. In contrast, the $3\tilde{C}$ model allows the height and width of the binary peak to be brought into greater agreement with both the experiment [4,7] and the results obtained by both the perturbative [4] and ab initio [18] methods.

This numerical investigation confirms the effectiveness of the developed approach in the kinematic regimes under consideration. Therefore, further development beyond the $3\tilde{C}$ model holds good promise.

Author Contributions: Conceptualization, S.A.Z., Y.V.P., L.U.A. and K.A.K.; methodology, S.A.Z., Y.V.P., L.U.A. and K.A.K.; software, A.S.Z., D.S.Z. and S.A.Z.; formal analysis, S.A.Z., Y.V.P., L.U.A. and K.A.K.; writing—original draft preparation, S.A.Z.; writing—review and editing, L.U.A., Y.V.P. and K.A.K. All authors have read and agreed to the published version of the manuscript.

Funding: This work is supported by the Ministry of Science and Higher Education of the Russian Federation (project no. FEME-2024-0005). The work of S.A.Z. was supported by the Russian Science Foundation under grant no. 24-22-20047, https://rscf.ru/en/project/24-22-20047/ URL (accessed on

15 December 2025). Y.V.P. and K.A.K. disclose that this study was partially conducted under the state assignment of Lomonosov Moscow State University.

Data Availability Statement: The original contributions presented in this study are included in the article. Further inquiries can be directed to the corresponding author.

Acknowledgments: The research is carried out using the equipment of the Shared Facility Center "Data Center of FEB RAS" (Khabarovsk, Russia) [31].

Conflicts of Interest: The authors declare no conflicts of interest.

Abbreviations

The following abbreviations are used in this manuscript:

FDCS	Fully differential cross-section
DI	Direct ionization
ECC	Electron capture to the continuum
LS	Lippmann–Schwinger equation
2C	Two-Coulomb wave
3C	Three-Coulomb wave
CQS	Convolution of quasi-Sturmian

References

1. Maydanyuk, N.V.; Hasan, A.; Foster, M.; Tooke, B.; Nanni, E.; Madison, D.H.; Schulz, M. Projectile-residual-target-ion scattering after single ionization of helium by slow proton impact. *Phys. Rev. Lett.* **2005**, *94*, 243201. [CrossRef]
2. Schulz, M.; Madison, D.H. Studies of the few-body problem in atomic break-up processes. *Int. J. Mod. Phys. A* **2006**, *21*, 3649. [CrossRef]
3. Schulz, M.; Hasan, A.; Maydanyuk, N.V.; Foster, M.; Tooke, B.; Madison, D.H. Kinematically complete experiment on single ionization in 75-keV p+He collisions. *Phys. Rev. A* **2006**, *73*, 062704. [CrossRef]
4. Dhital, M.; Bastola, S.; Silvus, A.; Lamichhane, B.R.; Ali, E.; Ciappina, M.F.; Lomsadze, R.; Hasan, A.; Madison, D.H.; Schulz, M. Target dependence of postcollision interaction effects on fully differential ionization cross sections. *Phys. Rev. A* **2019**, *100*, 032707. [CrossRef]
5. Dhital, M.; Bastola, S.; Silvus, A.; Davis, J.; Lamichhane, B.R.; Ali, E.; Ciappina, M.F.; Lomsadze, R.; Hasan, A.; Madison, D.H.; et al. Ejected-electron-energy and angular dependence of fully differential ionization cross sections in medium-velocity proton collisions with He and H_2. *Phys. Rev. A* **2020**, *102*, 032818. [CrossRef]
6. Bastola, S.; Dhital, M.; Majumdar, S.; Hasan, A.; Lomsadze, R.; Davis, J.; Lamichhane, B.; Borbély, S.; Nagy, L.; Schulz, M. Interference effects in fully differential ionization cross sections near the velocity vatching in p+He collisions. *Atoms* **2022**, *10*, 119. [CrossRef]
7. Majumdar, S.; Bastola, S.; Hasan, A.; Lomsadze, R.; Schulz, M. Separation of various higher-order effects in the ionization of helium by proton impact. *Phys. Rev. A* **2024**, *110*, 032814. [CrossRef]
8. Abdurakhmanov, I.B.; Kadyrov, A.S.; Alladustov, S.U.; Bray, I.; Bartschat, K. Fully differential cross sections for single ionization of helium by energetic protons. *Phys. Rev. A* **2019**, *100*, 062708. [CrossRef]
9. Zaytsev, A.S.; Zaytseva, D.S.; Zaytsev, S.A.; Ancarani, L.U.; Kouzakov, K.A. Parabolic quasi-Sturmian approach to proton-impact ionization of helium. *Phys. Rev. A* **2022**, *105*, 062818. [CrossRef]
10. Walters, H.R.J.; Whelan, C.T. Differential ionization of a one-electron target under bare-ion impact: Application to proton-impact ionization of atomic hydrogen. *Phys. Rev. A* **2015**, *92*, 062712. [CrossRef]
11. Abdurakhmanov, I.B.; Bailey, J.J.; Kadyrov, A.S.; Bray, I. Wave-packet continuum-discretization approach to ion-atom collisions including rearrangement: Application to differential ionization in proton-hydrogen scattering. *Phys. Rev. A* **2018**, *97*, 032707. [CrossRef]
12. Zaytsev, S.; Zaytsev, A.; Kramar, E.; Ancarani, L.U.; Popov, Y.; Kouzakov, K. Single ionization of helium by 75 keV protons outside the velocity-matching regime in the parabolic quasi-Sturmian approach. *Eur. Phys. J. D* **2025**, *79*, 55. [CrossRef]
13. Zaytsev, S.A.; Zaytseva, D.S.; Zaytsev, A.S.; Ancarani, L.U.; Kouzakov, K.A.; Popov, Y.V. Quasi-Sturmian basis set for problems of single ionization of helium by proton impact with rearrangement. *Phys. Rev. A* **2025**, *111*, 052812. [CrossRef]
14. Popov, Y.V.; Zaytsev, S.A.; Kouzakov, K.A.; Ancarani, L.U. Single Ionization of Helium Atom by 75 keV Protons Near the Cusp Region. In *Reviews of Light and Heavy Particle Collisions with Atoms and Molecules*; Belkić, D., Ed.; World Scientific: Singapore, 2026; pp. 207–226.

15. Merkur'ev, S.P. Integral equations in the quantum scattering problem for a system of three charged particles. *Theor. Math. Phys.* **1979**, *38*, 134–145. [CrossRef]
16. Garibotti, C.R.; Miraglia, J.E. Ionization and electron capture to the continuum in the H^+-hydrogen-atom collision. *Phys. Rev. A* **1980**, *21*, 572. [CrossRef]
17. Brauner, M.; Briggs, J.S.; Klar, H. Triply-differential cross sections for ionisation of hydrogen atoms by electrons and positron. *J. Phys. B At. Mol. Opt. Phys.* **1989**, *21*, 2265. [CrossRef]
18. Spicer, K.H.; Antonio, N.W.; Schöffler, M.S.; Schulz, M.; Kadyrov, A.S. Coupled-channel calculations of fully differential cross sections for ionization in 75-keV p + He collisions. *Phys. Rev. A* **2025**, *112*, 032806. [CrossRef]
19. Klar, H. Asymptotic separability of three-body continuum wave functions for Coulomb systems. *Z. Phys. D At. Mol. Clust.* **1990**, *16*, 231.
20. Merkuriev, S.P.; Faddeev, L.D. *Quantum Scattering Theory for Several Particle Systems*, 1st ed.; Springer: Dordrecht, The Netherlands, 1993.
21. Ojha, P.C. The Jacobi-matrix method in parabolic coordinates: Expansion of Coulomb functions in parabolic Sturmians. *J. Math. Phys.* **1987**, *28*, 392. [CrossRef]
22. Zaytsev, S.A.; Ancarani, L.U.; Zaytsev, A.S.; Kouzakov, K.A. A parabolic quasi-Sturmian approach to quantum scattering by a Coulomb-like potential. *Eur. Phys. J. Plus* **2020**, *135*, 655. [CrossRef]
23. Buchholz, H. *The Confluent Hypergeometric Function*; Springer: Berlin/Heidelberg, Germany, 1969.
24. Zaytsev, A.S.; Zaytseva, D.S.; Ancarani, L.U.; Zaytsev, S.A. Double ionization of helium with a convoluted quasi Sturmian approach. *Eur. Phys. J. D* **2019**, *73*, 111. [CrossRef]
25. Ciappina, M.F.; Cravero, W.R.; Schulz, M. Post-collisional effects on single ionization in 75 keV p+He collisions. *J. Phys. B At. Mol. Opt. Phys.* **2007**, *40*, 2577. [CrossRef]
26. Ma, X.Y.; Li, X.; Sun, S.Y.; Jia, X.F. Structures in fully differential cross-sections for proton-impact ionization of helium. *Europhys. Lett.* **2012**, *98*, 53001. [CrossRef]
27. Ghanbari-Adivi, E.; Eskandari, S. Electron correlation in fast ion-impact single ionization of helium atoms. *Chin. Phys. B* **2015**, *24*, 013401. [CrossRef]
28. Duan, Y.H.; Sun, S.Y.; Jia, X.F. Internuclear interaction on fully differential cross-sections for single ionization of helium by proton impact. *Europhys. Lett.* **2015**, *110*, 13001. [CrossRef]
29. Niu, X.; Sun, S.; Wang, F.; Jia, X. Dynamic correlation effects in fully differential cross sections for 75-keV proton-impact ionization of helium. *Phys. Rev. A* **2017**, *96*, 022703. [CrossRef]
30. Zaytsev, A.S.; Zaytseva, D.S.; Zaytsev, S.A.; Ancarani, L.U.; Chuluunbaatar, O.; Kouzakov, K.A.; Popov, Y.V. Single Ionization of Helium by Protons of Various Energies in the Parabolic Quasi-Sturmians Approach. *Atoms* **2023**, *11*, 124. [CrossRef]
31. Sorokin, A.A.; Makogonov, S.V.; Korolev, S.P. The Information Infrastructure for Collective Scientific Work in the Far East of Russia *Sci. Tech. Inf. Process.* **2017**, *44*, 302. [CrossRef]

Disclaimer/Publisher's Note: The statements, opinions and data contained in all publications are solely those of the individual author(s) and contributor(s) and not of MDPI and/or the editor(s). MDPI and/or the editor(s) disclaim responsibility for any injury to people or property resulting from any ideas, methods, instructions or products referred to in the content.